05.5

A weakly-tunable transmon qubit with an optimized shape of the shunted capacitance

© E.Yu. Egorova[1–3], A.S. Kazmina[1–3], I.N. Moskalenko[2]

[1] Russian Quantum Center, Moscow, Russia
[2] National University of Science and Technology„MISiS“, Moscow, Russia
[3] Moscow Institute of Physics and Technology (National Research University), Dolgoprudny, Moscow Region, Russia
E-mail: yelena.egorova@phystech.edu

Received September 18, 2023
Revised November 10, 2023
Accepted November 10, 2023

An optimized transmon topology is proposed as a base element in a superconducting quantum processor. An analytical formula is obtained for the energy levels of a transmon with three Josephson junctions. It is shown that the three-junction transmon makes it possible to obtain a narrower frequency tunability range in comparison to a two-junction transmon with comparable sizes of Josephson junctions in the structure, that reduces sensitivity to flux noise. Electromagnetic modeling of electric field distribution on technological surfaces is carried out. It is shown that the round shape of the shunted capacitance of the transmon reduces the dielectric losses at the interfaces compared to the most common cross shape.

Keywords: transmon qubit, Josephson junctions, technological interfaces.

DOI: 10.21883/0000000000

Transmon [1] — is one of the most common qubit types in the modern superconducting schemes. Currently, quantum computations, execution of quantum algorithms and quantum error correction are made by using multiqubit schemes consisting of interacting transmons [2,3]. Because of the shunted capacitance, the sensitivity to low-frequency charge noise in such qubits is suppressed. Also, the transmons have lower susceptibility to flux noises compared to the flux qubits [4]. Moreover, the transmons have no Josephson junction arrays required in the creation of fluxonium qubits [5], which makes them relatively more simple in the fabrication. The transmons have sufficient coherency times for the implementation of sets of quantum gates [6] used in the quantum data processing algorithms. The most common type of transmons — is the tunable X-mon [7], having crosswise shunted capacitance and two Josephson junctions forming a superconducting quantum interferometer (SQUID), which provides qubit tunability by frequency.

Today, the most significant reason for the limitation of the coherency time of transmon qubits is dielectric losses associated with the two-level defects near to the vacuum−substrate and metal−substrate interfaces, as well as inside the Josephson junction barrier [8–11]. At the same time, in the regions with high density of the electric field energy such defects can be strongly coupled with qubit and their number is quite low, so it is possible to observe individual qubit resonances with individual defects [12]. An important indicator is the participation ratio of the interfaces, i.e. the ratio of the electric field energy in the volume that contains such defects to the total electric field energy of the qubit.

Regardless of a wide range of the transmons frequency tunability, obtaining high coherency times is limited by the flux noise. Due to a low-frequency flux noise, high coherency times are only possible in the frequency extrema as functions of flux in SQUID, where the qubit frequency derivative with respect to the magnetic field is zero. Therefore, the qubit in the first approximation is non-sensitive to flux noise [13].

Thus, design of transmon qubit topology with high coherency times requires decrease of the participation ratios of the interfaces with defects. On the other hand, the minimum size of Josephson junctions is limited by reproducibility of their fabrication.

In this study we propose optimized transmon qubit with single Josephson junction and SQUID connected in series [14], as well as with the round shape of the shunted capacitance [15–17]. The topology of such qubit and its equivalent electrical scheme are given in Fig. 1. The round shunted capacitance C_2 (red color) is associated with the ground (black color) via a circuit of three Josephson junctions J_1 , J_2 , J_3 with own capacitances $C_{J1,2}$ and C_{J3} (green color). A control line for the qubit control is laid to the transmon's SQUID. Yellow color denotes electrodes of the qubit's capacitive coupling with the other possible elements in the scheme.

Hamiltonian of the three-junction transmon is derived from the description of classical dynamics of the electromagnetic circuits [18]:

$$\widehat{H}_{tr} = 4E_C\widehat{n}^2 + E_{J3}(1-\cos\widehat{\varphi}_2) + E_{J12}\cos(\pi\Phi/\Phi_0) \times \sqrt{1+d^2\tan^2(\pi\Phi/\Phi_0)}(1-\cos\widehat{\varphi}_1), \quad (1)$$

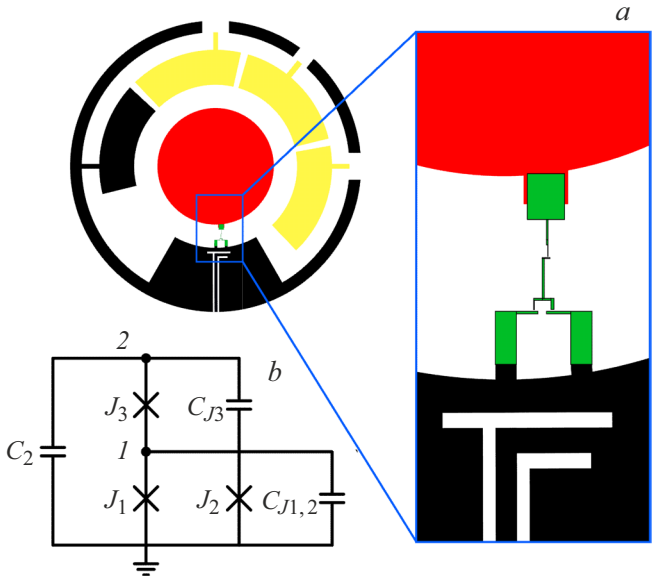

Figure 1. *a* — transmon topology with the round shunted capacitance (red color). Inset — Zoomed-in image of a single Josephson junction serially connected to SQUID (green color). External magnetic flux is applied to SQUID through inductively coupled control line (black color). Yellow color denotes electrodes — the arcs of the capacitive coupling with the other potential elements of the system. A color version of the Figure is provided in the online version of the paper. *b* — equivalent electrical scheme of the three-junction transmon. The digits denote electrical nodes of the circuit: *1* — a node between single Josephson junction J_3 with own capacitance C_{J3} and SQUID with Josephson junctions J_1 and J_2 with the total capacitance $C_{J1,2}$, *2* — the node of the shunted capacitance C_2 to the ground.

where $\widehat{\varphi}_2$ — phase operator on the Josephson junction J_3, $\widehat{\varphi}_1$ — phase operator on the Josephson junction J_1, $\widehat{n}$ — operator of the number of Cooper pairs, which is canonically conjugated with the sum of the operators $\widehat{\varphi} = \widehat{\varphi}_1 + \widehat{\varphi}_2$. Here E_C — charge energy of transmon, $E_{J12} = E_{J1} + E_{J2}$ — total Josephson energy of two junctions with SQUID, $d = (E_{J2} - E_{J1})/(E_{J1} + E_{J2})$ — SQUID asymmetry, Φ — external magnetic flux to SQUID, $\Phi_0 = h/2e$ — magnetic flux quantum.

The analytical formula for the energy levels of that transmon and its anharmonicity can be obtained in the similar way [1] by decomposing the cosine into Taylor's series up to the fourth order due to smallness φ in the mode $E_C/E_{Js} \ll 1$ [19]:

$$\widehat{H}_{tr} = 4E_C\widehat{n}^2 + \frac{1}{2}E_{Js}\widehat{\varphi}^2 - \frac{1}{24}E_{Jq}\widehat{\varphi}^4, \qquad (2)$$

where $E_{Js} = E_{J3}\tilde{E}_{J12}/(E_{J3} + \tilde{E}_{J12})$ — linear part of the inductive energy, $E_{Jq} = (E_{J3}^4\tilde{E}_{J12} + E_{J3}\tilde{E}_{J12}^4)/(E_{J3} + \tilde{E}_{J12})^4$ — quadratic part. Here we introduced the notation $\tilde{E}_{J12} = E_{J12}\cos(\pi\Phi/\Phi_0)\sqrt{1 + d^2\tan^2(\pi\Phi/\Phi_0)}$ for the Josephson energy of SQUID that depends on the external magnetic flux. In deriving the formula we used approximation for the serial connection of single Josephson junction and SQUID, in which the currents of the Josephson contacts are decomposing into the Taylor's series up to the first order due to the smallness of the phases of the junctions: $\varphi_1\tilde{E}_{J12} = \varphi_2 E_{J3}$.

By using the first order of the perturbations theory for that Hamiltonian, the levels of energies for a three-junction transmon can be written as

$$E_m = \sqrt{8E_CE_{Js}}\left(m + \frac{1}{2}\right) - E_C\frac{E_{Jq}}{12E_{Js}}\left(6m^2 + 6m + 3\right), \qquad (3)$$

which results in the qubit frequency f_{01} and anharmonicity α respectively

$$f_{01} = \left(\sqrt{8E_CE_{Js}} - E_C\frac{E_{Jq}}{E_{Js}}\right)\Big/h, \qquad (4)$$

$$\alpha = E_{12} - E_{01} = -E_C\frac{E_{Jq}}{E_{Js}}. \qquad (5)$$

Fig. 2 represents the range of tunability of the qubit frequency and its anharmonicity according to analytical formulas (4) and (5) depending on the external magnetic flux to SQUID. The calculation was performed by using the data from Table 1. With sufficient anharmonicity the range of tunability of frequency of the three-junction transmon is narrower than that for two-junction ones [20], which makes it more useful in multiqubit schemes.

Since dielectric losses make a contribution into the inverse Q factor of qubit [21], which, in turn, affects the qubit relaxation rate due to the ratio $\gamma_1 = \omega Q^{-1}$, we performed simulation and calculation by means of Ansys

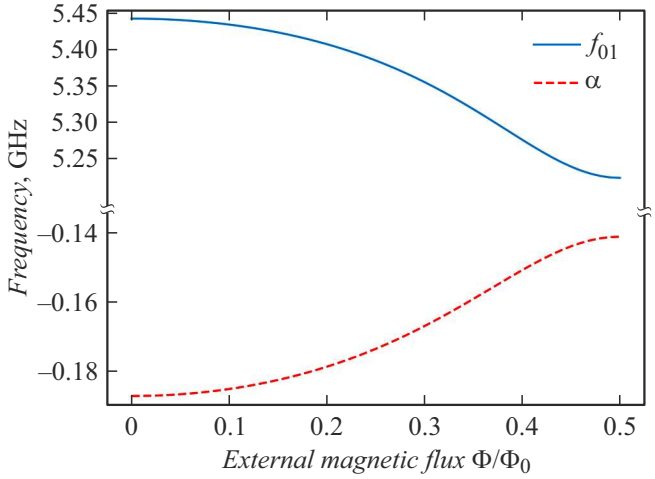

Figure 2. Frequency of qubit and anharmonicity, depending on the magnetic flux in SQUID, obtained according to analytical formulas (4) and (5) for the three-junction transmon.

Table 1. Transmon parameters: Josephson energies of junctions and charge energy

E_{J1}, GHz	E_{J2}, GHz	E_{J3}, GHz	E_C, MHz
124.2	43.5	17.4	251

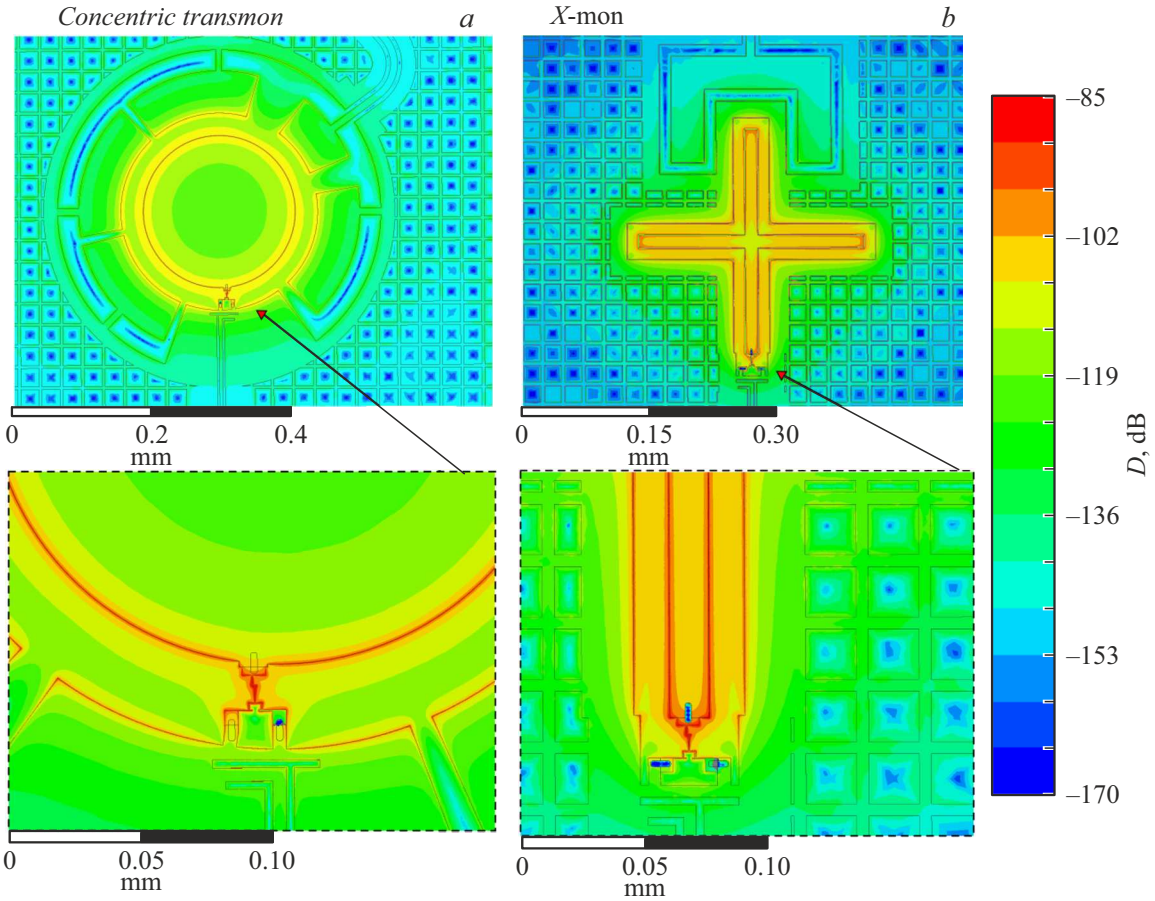

Figure 3. Simulation of distribution of the electrical field by using the Ansys HFSS software in transmons with different shape of the shunted capacitance. *a* — transmon with the round capacitance (concentric transmon), *b* — transmon with the crosswise capacitance (*X*-mon). Zoomed-in regions with the Josephson junctions are shown below. Color denotes the value of electric displacement field on the surface (D) in Decibells. A color version of the Figure is provided in the online version of the paper.

Table 2. Integrals of the energy of the electrical field on the surfaces, expressed in relative units, obtained in the Ansys HFSS software (simulation was performed by using three types of the surfaces: ms-o — metal–substrate in the base layer of photolithography, ms-e — metal–substrate for the electron-beam lithography, sa — surface of the silica substrate)

Qubit type	Interface		
	ms-e	ms-o	sa
Concentric transmon	3.92	17.2	30.4
X-mon	3.61	46.9	78.9

HFSS software for the participation ratio of electrical field in the technological interfaces for two shapes of the shunted capacitances of the same value in transmon.

The contribution of dielectric losses into the qubit Q factor is described by the ratio $Q^{-1} = \Sigma_i p_i \tan\delta_i$, where p_i — participation ratio of the surface energy of the electrical field at the i-th technological interface, $\tan\delta_i$ — tangent of dielectric losses angle. Surfacel energy of electrical field is represented as the integral of energy of the electrical field on the i-th surface $\int |E^2| dS_i$.

The first type of transmon has the round capacitance, the second one — crosswise. Both qubits include three Josephson junctions. The simulation involves three types of interfaces: metal–substrate in the base layer of photolithography (ms-o), metal–substrate for the layer of electron-beam lithography (ms-e) and the surface of silicon substrate (sa). Electron-beam lithography is intended for the manufacture of Josephson junctions having the size lower than $1\,\mu$m. The simulation did not consider the interface metal–air, since the field participation ratio therein is negligibly small relative to the interface metal–substrate [9]. The superconductor is simulated as an ideal conductor, which simplifies the calculation, because the contribution of kinetic inductance is not considered. The simulation region is limited to 1 mm perpendicularly to the substrate surface. The obtained distribution of the electric field is shown in Fig. 3, *a* and *b* for concentric transmon and *X*-mon, respectively. Final participation ratios of the interfaces are given in Table 2. Compared to *X*-mon, the concentric

one has a lower energy in the substrate (sa) and in the photolithography interface metal−substrate (ms-o).

In addition to the minimization of dielectric losses, in Ansys HFSS we assessed the relaxation of the concentric transmon into the control line. For that purpose we introduced the boundary condition for the flux line as a matched load (50 Ω), and the Josephson junctions were simulated as linearized equivalent of lumped inductances. The same as for the participation ratio calculation, in this one the thickness of the silicon substrate and the air layer above the metal are 0.5 mm. The simulation results have shown that the upper limit for the qubit relaxation time at the point with the maximum frequency to that channel is 1.6 ms.

Thus, the proposed topology of transmon with the round capacitance has a series of advantages versus *X*-mon, namely, a narrow frequency tunability range with sufficient anharmonicity and lower dielectric losses on the technological surfaces.

Acknowledgments

The authors express gratitude to I.S. Besedin and A.V. Ustinov for the proposed ideas and fruitful discussions.

Funding

The research was carried out within the framework of Russian Roadmap on Quantum Computing (Contract No. 151/21-503, December 21, 2021 dated 12/21/2021).

Conflict of interest

The authors declare that they have no conflict of interest.

References

[1] J. Koch, T.M. Yu, J. Gambetta, A.A. Houck, D.I. Schuster, J. Majer, A. Blais, M.H. Devoret, S.M. Girvin, R.J. Schoelkopf, Phys. Rev. A, **76** (4), 042319 (2007). DOI: 10.1103/PhysRevA.76.042319

[2] F. Arute, K. Arya, R. Babbush, D. Bacon, J.C. Bardin, R. Barends, R. Biswas, S. Boixo, F.G.S.L. Brandao, D.A. Buell, B. Burkett, Y. Chen, Z. Chen, B. Chiaro, R. Collins, W. Courtney, A. Dunsworth, E. Farhi, B. Foxen, A. Fowler, C. Gidney, M. Giustina, R. Graff, K. Guerin, S. Habegger, M.P. Harrigan, M.J. Hartmann, A. Ho, M. Hoffmann, T. Huang, T.S. Humble, S.V. Isakov, E. Jeffrey, Z. Jiang, D. Kafri, K. Kechedzhi, J. Kelly, P.V. Klimov, S. Knysh, A. Korotkov, F. Kostritsa, D. Landhuis, M. Lindmark, E. Lucero, D. Lyakh, S. Mandrá, J.R. McClean, M. McEwen, A. Megrant, X. Mi, K. Michielsen, M. Mohseni, J. Mutus, O. Naaman, M. Neeley, C. Neill, M.Y. Niu, E. Ostby, A. Petukhov, J.C. Platt, C. Quintana, E.G. Rieffel, P. Roushan, N.C. Rubin, D. Sank, K.J. Satzinger, V. Smelyanskiy, K.J. Sung, M.D. Trevithick, A. Vainsencher, B. Villalonga, T. White, Z.J. Yao, P. Yeh, A. Zalcman, H. Neven, J.M. Martinis, Nature, **574** (7779), 505 (2019). DOI: 10.1038/s41586-019-1666-5

[3] C.K. Andersen, A. Remm, S. Lazar, S. Krinner, N. Lacroix, G.J. Norris, M. Gabureac, C. Eichler, A. Wallraff, Nat. Phys., **16** (8), 875 (2020). DOI: 10.1038/s41567-020-0920-y

[4] F. Yan, S. Gustavsson, A. Kamal, J. Birenbaum, A.P. Sears, D. Hover, T.J. Gudmundsen, D. Rosenberg, G. Samach, S. Weber, J.L. Yoder, T.P. Orlando, J. Clarke, A.J. Kerman, W.D. Oliver, Nat. Commun., **7** (1), 12964 (2016). DOI: 10.1038/ncomms12964 (2016)

[5] L.B. Nguyen, Y.-H. Lin, A. Somoroff, R. Mencia, N. Grabon, V.E. Manucharyan, Phys. Rev. X, **9** (4), 041041 (2019). DOI: 10.1103/PhysRevX.9.041041

[6] Z. Li, P. Liu, P. Zhao, Z. Mi, H. Xu, X. Liang, T. Su, W. Sun, G. Xue, J.-N. Zhang, W. Liu, Y. Jin, H. Yu, *Error per single-qubit gate below* 10^{-4} *in a superconducting qubit*, arXiv:2302.08690 (2023). DOI: 10.48550/arXiv.2302.08690

[7] R. Barends, J. Kelly, A. Megrant, D. Sank, E. Jeffrey, Y. Chen, Y. Yin, B. Chiaro, J. Mutus, C. Neill, P. O'Malley, P. Roushan, J. Wenner, T.C. White, A.N. Cleland, J.M. Martinis, Phys. Rev. Lett., **111** (8), 080502 (2013). DOI: 10.1103/PhysRevLett.111.080502

[8] C. Wang, C. Axline, Y.Y. Gao, T. Brecht, Y. Chu, L. Frunzio, M.H. Devoret, R.J. Schoelkopf, Appl. Phys. Lett., **107** (16), 162601 (2015). DOI: 10.1063/1.4934486

[9] J. Wenner, R. Barends, R.C. Bialczak, Y. Chen, J. Kelly, E. Lucero, M. Mariantoni, A. Megrant, P.J.J. O'Malley, D. Sank, A. Vainsencher, H. Wang, T.C. White, Y. Yin, J. Zhao, A.N. Cleland, J.M. Martinis, Appl. Phys. Lett., **99** (11), 113513 (2011). DOI: 10.1063/1.3637047

[10] J.M. Gambetta, C.E. Murray, Y.-K.-K. Fung, D.T. McClure, O. Dial, W. Shanks, J.W. Sleight, M. Steffen, IEEE Trans. Appl. Supercond., **27** (1), 1700205 (2017). DOI: 10.1109/TASC.2016.2629670

[11] J.M. Martinis, K.B. Cooper, R. McDermott, M. Steffen, M. Ansmann, K.D. Osborn, K. Cicak, S. Oh, D.P. Pappas, R.W. Simmonds, C.C. Yu, Phys. Rev. Lett., **95** (21), 210503 (2005). DOI: 10.1103/PhysRevLett.95.210503

[12] J. Lisenfeld, G.J. Grabovskij, C. Müller, J.H. Cole, G. Weiss, A.V. Ustinov, Nat. Commun., **6**, 6182 (2015). DOI: 10.1038/ncomms7182

[13] J. Braumüller, L. Ding, A.P. Vepsäläinen, Y. Sung, M. Kjaergaard, T. Menke, R. Winik, D. Kim, B.M. Niedzielski, A. Melville, J.L. Yoder, C.F. Hirjibehedin, T.P. Orlando, S. Gustavsson, W.D. Oliver, Phys. Rev. Appl., **13** (5), 054079 (2020). DOI: 10.1103/PhysRevApplied.13.054079

[14] J.M. Chávez-Garcia, F. Solgun, J.B. Hertzberg, O. Jinka, M. Brink, B. Abdo, Phys. Rev. Appl., **18** (3), 034057 (2022). DOI: 10.48550/arXiv.2203.04164

[15] J. Braumüller, M. Sandberg, M.R. Vissers, A. Schneider, S. Schlör, L. Grünhaupt, H. Rotzinger, M. Marthaler, A. Lukashenko, A. Dieter, A.V. Ustinov, M. Weides, D.P. Pappas, Appl. Phys. Lett., **108** (3), 032601 (2016). DOI: 10.1063/1.4940230

[16] J. Rahamim, T. Behrle, M.J. Peterer, A. Patterson, P.A. Spring, T. Tsunoda, R. Manenti, G. Tancredi, P.J. Leek, Appl. Phys. Lett., **110** (22), 222602 (2017). DOI: 10.1063/1.4984299

[17] S.A. Caldwell, N. Didier, C.A. Ryan, E.A. Sete, A. Hudson, P. Karalekas, R. Manenti, M.P. da Silva, R. Sinclair, E. Acala, N. Alidoust, J. Angeles, A. Bestwick, M. Block, B. Bloom, A. Bradley, C. Bui, L. Capelluto, R. Chilcott, J. Cordova, G. Crossman, M. Curtis, S. Deshpande, T. El Bouayadi, D. Girshovich, S. Hong, K. Kuang, M. Lenihan,

T. Manning, A. Marchenkov, J. Marshall, R. Maydra, Y. Mohan, W. O'Brien, C. Osborn, J. Otterbach, A. Papageorge, J.-P. Paquette, M. Pelstring, A. Polloreno, G. Prawiroatmodjo, V. Rawat, M. Reagor, R. Renzas, N. Rubin, D. Russell, M. Rust, D. Scarabelli, M. Scheer, M. Selvanayagam, R. Smith, A. Staley, M. Suska, N. Tezak, D.C. Thompson, T.-W. To, M. Vahidpour, N. Vodrahalli, T. Whyland, K. Yadav, W. Zeng, C. Rigetti, Phys. Rev. Appl., **10** (3), 034050 (2018). DOI: 10.1103/PhysRevApplied.10.034050

[18] U. Vool, M. Devoret, Int. J. Circuit Theory Appl., **45** (7), 897 (2017). DOI: 10.1002/cta.2359

[19] S.M. Girvin, in *Quantum machines: measurement and control of engineered quantum systems* (Oxford University Press, 2014), p. 113–256. DOI: 10.1093/acprof:oso/9780199681181.003.0003

[20] M.D. Hutchings, J.B. Hertzberg, Y. Liu, N.T. Bronn, G.A. Keefe, M. Brink, J.M. Chow, B.L.T. Plourde, Phys. Rev. Appl., **8** (4), 044003 (2017). DOI: 10.1103/PhysRevApplied.8.044003

[21] A. Dunsworth, A. Megrant, C. Quintana, Z. Chen, R. Barends, B. Burkett, B. Foxen, Y. Chen, B. Chiaro, A. Fowler, R. Graff, E. Jeffrey, J. Kelly, E. Lucero, J.Y. Mutus, M. Neeley, C. Neill, P. Roushan, D. Sank, A. Vainsencher, J. Wenner, T.C. White, J.M. Martinis, Appl. Phys. Lett., **111** (2), 022601 (2017). DOI: 10.1063/1.4993577

Translated by D.Kondaurov